Review

The structure of the H^+-ATP synthase from chloroplasts and its subcomplexes as revealed by electron microscopy

Bettina Böttcher [a], Peter Gräber [b],*

[a] *European Molecular Biology Laboratory, Heidelberg, Meyerhofstrasse 1, Postfach 102209, 69012 Heidelberg, Germany*
[b] *Institut für Physikalische Chemie, Albertstrasse 23a, 79104 Freiburg, Germany*

Abstract

The electron microscopic data available on CF_0F_1 and its subcomplexes, CF_0, CF_1, subunit III complex are collected and the CF_1 data are compared with the high resolution structure of MF_1. The data are based on electron microscopic investigation of negatively stained isolated CF_1, CF_0F_1 and subunit III complex. In addition, two-dimensional crystals of CF_0F_1 and CF_0F_1 reconstituted liposomes were investigated by cryo-electron microscopy. Progress in the interpretation of electron microscopic data from biological samples has been made with the introduction of image analysis. Multi-reference alignment and classification of images have led to the differentiation between different conformational states and to the detection of a second stalk. Recently, the calculation of three-dimensional maps from the class averages led to the understanding of the spatial organisation of the enzyme. Such three-dimensional maps give evidence of the existence of a third connection between the F_0 part and F_1 part. © 2000 Elsevier Science B.V. All rights reserved.

Keywords: Chloroplast; H^+-ATPase; Adenosine triphosphate synthase; H^+-translocating ATPase from chloroplast; Electron microscopy

1. Introduction

H^+-ATPases ('ATP synthase', 'F-type ATPase', 'F_0F_1') catalyse proton transport coupled with ATP synthesis and ATP hydrolysis in bacteria, chloroplasts and mitochondria, i.e. they use the free enthalpy ('Gibb's free energy') derived from a transmembrane proton transport to synthesise the β-γ-phosphate bond in ATP from ADP and phosphate [1]. All F-type H^+-ATPases have a similar structure: they consist of a membrane-integrated, hydrophobic part, F_0, which contains the proton binding sites, and a hydrophilic part, F_1, which contains the nucleotide and phosphate binding sites.

The holoenzyme, F_0F_1, can be separated into the hydrophilic F_1 part and the hydrophobic F_0 part. The structures of the holoenzyme F_0F_1 and of the F_1 and F_0 parts have been investigated by electron microscopy. Since the structure of the F_1 moiety from mitochondria (MF_1) has been solved by X-ray diffraction to a resolution of 2.8 Å [2], this review is mainly focussed on the holoenzyme. F-type ATPases are multi-subunit enzymes showing differences in their subunit composition for enzymes from different sources. The H^+-ATPase from *Escherichia coli*, EF_0F_1, is the most simple one with eight different subunits, the most complex one is the enzyme from

mitochondria, MF_0F_1, with at least 13 different subunits. The H^+-ATPase from chloroplasts, CF_0F_1, has nine different subunits. An overview of the subunit compositions is given in Table 1. Homologous subunits are shown in the same row. The table also gives an overview for which subunit and subunit complex structural data are available and the method for structural determination.

The CF_1 part consists of five different subunits designated by Greek letters [3] with the stoichiometry $\alpha_3\beta_3\gamma\delta\epsilon$ [4,5]. The same subunit composition is found in EF_1. The CF_0 part consists of four different subunits designated by Roman numbers [6,7] with the likely stoichiometry I II III_{12} IV [7]. Subunits I and II are both homologous to the b-subunit in EF_0F_1, of which two copies are present. Subunit III forms a stable complex which can be isolated and is stable even in the presence of SDS. When CF_0F_1 was incubated in buffer containing SDS for 5 min at room temperature instead of 95°C before electrophoresis, subunit III was not observed at its 8 kDa position,

but an additional band corresponding to a molecular mass of approx. 100 kDa was found. It was concluded from the observed molecular masses that the 100 kDa complex contains 12 copies of subunit III [9]. However, it should be mentioned that this estimation is based on the electrophoretic mobility of the protein, and that the exact number of copies cannot be determined from these data. The reported stoichiometries of subunit III range between 6 and 12 [8,9]. The c-subunit of the H^+-ATPase from *E. coli* is homologous to subunit III and the chemically determined stoichiometry of subunit c in *E. coli* was 10 ± 1 [10]. Recent genetic fusion/cross-link experiments on the homologous subunit c of EF_0F_1 indicate that the exact number of copies is most likely 12 [11]. Subunit IV in CF_0F_1 was discovered rather late, since it is stained very weakly by Coomassie blue on a SDS-gel, and for a long time it was thought to be an impurity in the samples. After preparative gel electrophoresis and amino acid sequencing the sequence was compared with that deduced from the chloro-

Table 1
Stoichiometry of subunits and structural information on F-type H^+-ATPases and their subcomplexes

E. coli				Chloroplasts				Mitochondria			
Subunits (stoichiometry)		Structural data (method, Ref.)		Subunits (stoichiometry)		Structural data (method, Ref.)		Subunits (stoichiometry)		Structural data (method, Ref.)	
α	3			α	3			α	3		
β	3			β	3			β	3		
γ	1			γ	1			γ	1		
δ	1	NMR	[24]	δ	1			OSCP	1		
ϵ	1	NMR	[21,22]	ϵ	1			δ	1		
		X-ray	[23]								
–				–				ϵ	1		
EF_1		EM	[29–31]	CF_1		EM	[43–45]	MF_1		X-ray	[2,15–20]
										EM	[46–49]
a	1			IV	1			a	1		
b	2	NMR	[25]	I, II	1			b	2		
c	12	NMR	[26–28]	III	12	EM	[9]	c	12		
								d	1		
								F_6	1		
								e	1		
								f	1		
								g	1		
EF_0		AFM	[36,37]	CF_0				MF_0			
		EM	[35]								
EF_0F_1		EM	[32–34]	CF_0F_1		AFM	[38]	MF_0F_1		EM	[39,50–52]
						EM	[39–42]	IF_1	1		

Homologous subunits are given in the same rows. Subunit stoichiometries of the F_0 parts are estimated. IF_1 is the inhibitor protein of MF_0F_1. EM, electron microscopy; NMR, nuclear magnetic resonance; X-ray, X-ray diffraction; AFM, atomic force microscopy.
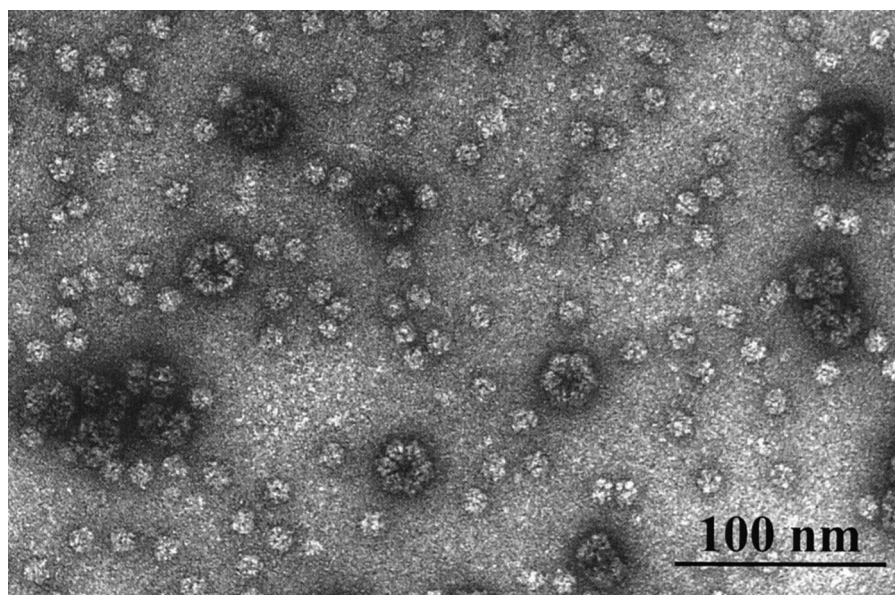
Fig. 1. Electron micrograph of negatively stained CF_1. CF_1 (small particles) was mixed with erythrocruorin (large particles) for optimal staining conditions [43].

plast gene *atpI* [12,13]. It turned out that the isolated subunit IV is identical to the gene derived sequence, the first 18 amino acids being removed before subunit IV is assembled into CF_0F_1 [7]. The amino acid sequence of subunit IV shows homologies with the a-subunit of *E. coli* [13].

All the existing structural information to near atomic resolution was either derived from MF_1 (0.28 nm resolution structure of $\alpha_3\beta_3\gamma$) or from single subunits of EF_0F_1 (NMR and X-ray of epsilon, NMR of c, NMR of parts of δ and parts of b). The structure of the holoenzyme is still unknown. Table 1 indicates that, at present, there are no high resolution data available on CF_0F_1, although there is a crystallisation note on CF_1 [14]. The only existing structural information on CF_0F_1 is of medium resolution and derives either from electron microscopic or atomic force microscopic investigations.

2. Structure of CF_1

The hydrophilic CF_1 part can be separated from the membrane-integrated CF_0 part [53]. Since no detergents are present in such F_1 preparations, the investigation of the F_1 parts is greatly facilitated. We have investigated the structure of isolated CF_1 by electron microscopy of negatively stained CF_1 [43].

The CF_1 complexes show distinct domains (see Fig. 1). Most of the molecules have a preferential orientation on the carbon support film. The resulting projections show a pseudo-hexagonal arrangement of domains. This view is called the hexagonal or top view. The low signal-to-noise ratio does not allow reliable interpretation of the finer details in an image of a single molecule. Therefore, the signal-to-noise ratio has been enhanced by averaging the images of similarly oriented molecules [54–57]. First, the electron micrograph is scanned with a densitometer and the light-dark pattern of the different molecule projections is measured. These digitised images are stored in a computer and one of the images is chosen as a first-reference molecule. The variance of the light-dark pattern of each image is normalised. Then, these images are oriented with regard to the reference molecule, i.e., they are rotated over an angle and also shifted translationally until the highest cross-correlation to the reference is obtained. Finally, the oriented images are added to give an average image, which now has an improved signal-to-noise ratio. This average image is then taken as a new reference image and the whole sequence is repeated until there is no further improvement. This procedure is carried out with different reference images ('image analysis'). In the case that the molecules do not have a preferential orientation or vary in their
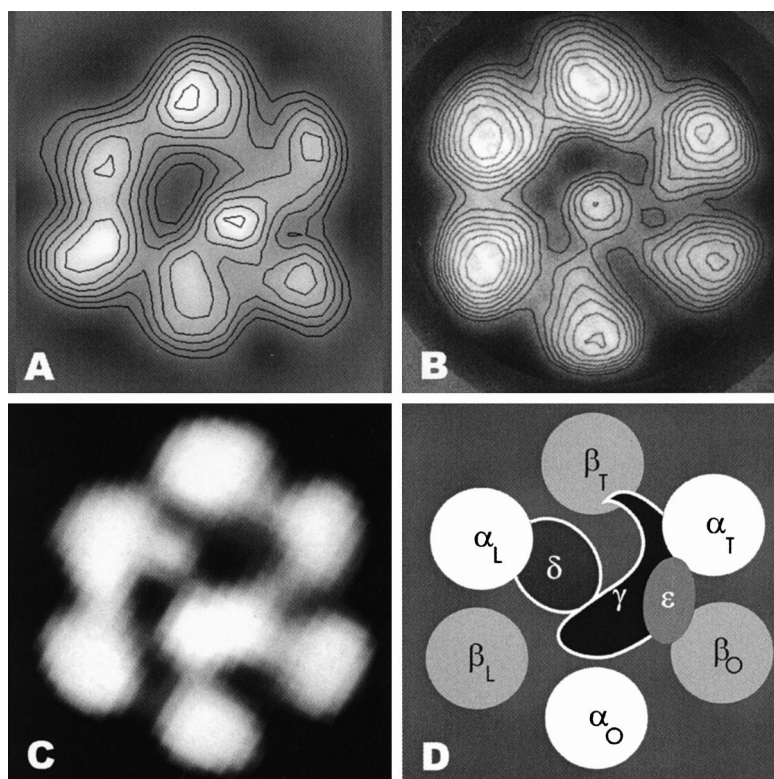
Fig. 2. Molecular projections of CF_1 and its interpretation. (A) Projection of the MF_1 X-ray structure [2] at the resolution level of the electron microscopic data, showing the positions of the α- and β-subunits and parts of the γ-subunit. (B) Class average from electron micrographs obtained with CF_1 without the ε- and δ-subunits [44,45]. (C) Class average from electron micrographs from CF_1 [43]. (D) Schematic interpretation of the electron microscopic data based on the MF_1 structure; T refers to β-subunit with bound AMPPNP, L to β-subunit with bound ADP, O to β-subunit without bound nucleotide.

functional states, averaging yields an image which does not correspond to a particular projection of the molecule and is therefore difficult to interpret. The differences between individual projections in the data set can be analysed by multivariate statistical techniques. This allows grouping of the molecule projections into different classes according to their similarity ('classification'). The images within the same class can then be averaged [54–57].

The images of 3300 CF_1 molecules were aligned and classified into 16 classes [43]. Fig. 2C shows one class from this data set. In order to interpret this structure the following comparisons were made. The atomic model of MF_1 derived from X-ray analysis shows the three α-subunits, the three β-subunits and parts of the γ-subunit [2]. For comparison to the electron microscopic data, this model was used to calculate a three-dimensional map. For simplicity, only the α-carbon atoms of the amino acids were included. The resulting three-dimensional map

was filtered suppressing information in the image with spatial frequencies smaller than $1/7.5$ nm^{-1} and larger than $1/2.2$ nm^{-1}. This creates a map which has a similar resolution and modulation of the contrast transfer function as observed in data derived from electron microscopy. The resulting three-dimensional map was then projected to give a similar hexagonal view as found by electron microscopy. This projection of MF_1 is shown in Fig. 2A. Since the MF_1 map contains no information about the localisation of the δ- and the ε-subunits, a projection map of CF_1 lacking these subunits [44,45] is shown in Fig. 2B. Both maps show a pseudo-hexagonal arrangement of densities surrounding a smaller density which is placed slightly out of the centre. The asymmetry of this arrangement allows a plausible assignment of the large densities in the original electron microscopic projection map and the projection map calculated from the atomic model of MF_1. A possible model is shown in Fig. 2D. The α- and β-

subunits are labelled according to the X-ray data. The position of the γ-subunit follows from the projection map of the atomic model and corresponds to the central density. The position of the ϵ-subunit and δ-subunits, which are missing in the atomic model, can be deduced from comparison of projection maps of CF_1 (Fig. 2C) and projection maps of CF_1 lacking either the ϵ-subunit, the δ-subunits or the ϵ- and δ-subunits (Fig. 2B).

3. Structure of CF_0

The shape of CF_0F_1 has been investigated by electron microscopy of detergent-solubilised enzyme after negative staining with uranyl acetate [39]. Fig. 3 shows a gallery of electron micrographs of CF_0F_1. Single CF_0F_1 molecules and different aggregates (*strings*) can be seen. Additionally, a schematic interpretation of the observed structure is given [39]. The F_0 parts (shaded areas) are strongly hydrophobic and, therefore, have a tendency to aggregate if not enough detergent is present. At the ends of each string detergent molecules presumably surround the hydrophobic parts. The F_1 parts are bigger than the F_0 parts and, therefore, the positions of F_1 will alter-

nate along the strings in order to avoid overlap. In Fig. 3 one can see that in most of the strings the F_1 parts of adjacent CF_0F_1 are alternating. The contours of the F_1 parts in the strings can be seen clearly. They are connected to the aggregated F_0 parts by a stalk. The thickness of the aggregated F_0 parts is 8.3 nm. For comparison, a typical bilayer membrane has a thickness of about 5 nm.

The dimensions of the F_0 part parallel to the strings cannot be measured directly from the micrographs as these parts stick tightly together and cannot be recognised as individual units. Additionally, detergent should be present at least at both ends of the strings. In such a case, the length of one F_0 part can be determined as follows: the length of well-preserved strings was measured and plotted versus the number of attached F_1 parts. Fig. 4, left, shows a plot of such data. The slope of this curve gives the increase in length of the string per CF_1. A length of 6.2 nm resulted and this represents the maximal dimension of the F_0 part along the string. If additional molecules (e.g. detergent, lipids) are present in the string, the diameter of F_0 is smaller. If the curve is extrapolated to zero, a value of 3.6 nm is obtained. This is exactly the length expected if octylglucoside (1.8 nm) surrounds both ends of the strings. It is,
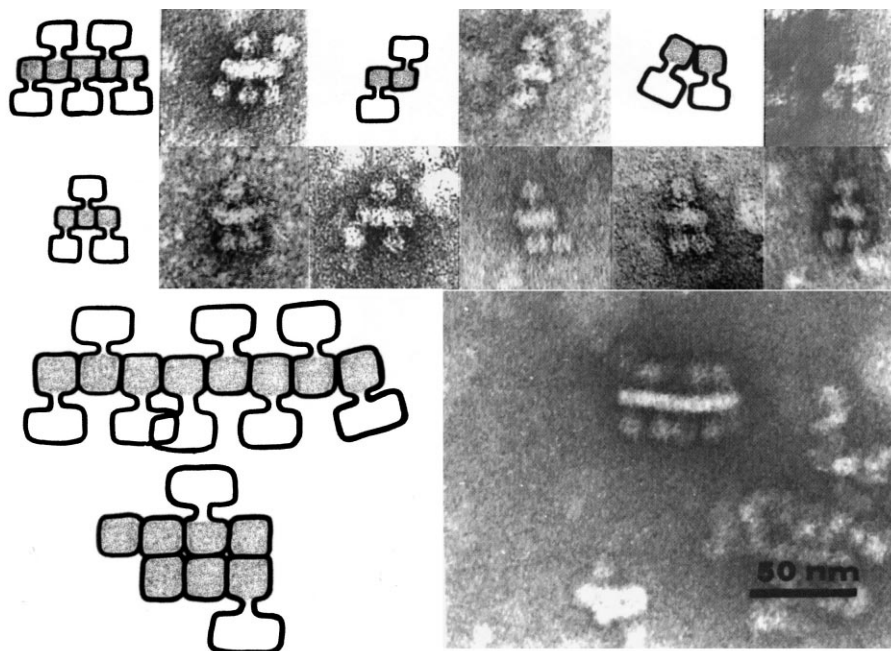

Fig. 3. Selected parts of electron micrographs of CF_0F_1 with schematic interpretation of its structure. The hydrophobic CF_0 parts of CF_0F_1 (shaded parts in the schemes) interact and form aggregates of different lengths. The number of attached CF_1 parts represents the minimal number of CF_0 parts of the aggregate [39].
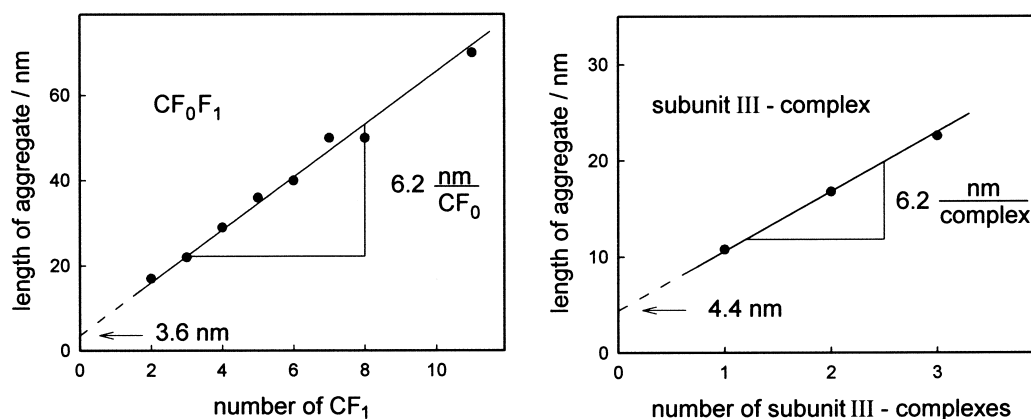
Fig. 4. Determination of the diameter of CF_0. (Left) The lengths of the aggregates shown in Fig. 3 are plotted as a function of the number of attached F_1 parts. The slope gives the aggregate length per CF_1, i.e., the maximal dimensions of CF_0 along the string axis [39]. (Right) The diameters of the subunit III stacks shown in Fig. 5 are plotted as a function of the number of complexes. The slope gives the minimal diameter per complex [9].

however, not clear from these results whether the F_0 part has a spherical or an elongated shape.

The hydrophobic CF_0 part can be isolated from the reconstituted CF_0F_1 [58]. It contains subunits I, II, III and IV. Electron microscopy of isolated CF_0 showed string-like structures. Presumably, these strings represent aggregates of CF_0 sticking together with their hydrophobic sides with an appearance similar to the hydrophobic parts of the strings shown in Fig. 3, shaded area. Individual molecules could not be distinguished (unpublished observations).

Subunit III forms an oligomeric complex with an apparent molecular mass of 100 kDa that was isolated by SDS-gel electrophoresis with subsequent electroelution of the gel. Fig. 5 shows the results of electron microscopic investigations of this complex [9]. The complex forms roll-like structures with up to 35 units of the 100 kDa complex arranged along the axis of one stack. The complexes are seen in a side-view projection perpendicular to their hydrophobic belt. The diameter of the stacks varies, indicating that one (Fig. 5, left, monomers), two (Fig. 5, centre dimers) or three (Fig. 5, right, trimers) complexes can form the repeating unit of a stack. At the bottom of Fig. 5 a schematic interpretation of the structure is depicted, and the different parameters are defined which can be measured: a_1, a_2 and a_3 are the diameters of the stack units, b is the repeating distance along the stack, c is the diameter of one 100 kDa subunit III complex, and d is the length of the detergent, in this case sodium dodecyl sulphate.

Fig. 4, right, shows a plot of the diameter of the stack units versus the number of units. From the slope of the curve the diameter c of one complex was calculated and it resulted in $c = 6.2$ nm. Extrapolation to zero gives 4.4 nm in agreement with the estimated thickness of the sodium dodecyl sulphate shell. The membrane spanning length b of the subunit III complex was 6.1 nm [9].

4. Structure of CF_0F_1

The electron microscopic investigations as reported above have been carried out on samples negatively stained with uranyl acetate. This method is fast and easy to use and results in micrographs with a high contrast. However, treatment with heavy-metal salts and drying of the sample do not ensure the preservation of a functionally and structurally intact enzyme. Embedding biological macromolecules by rapid freezing in a thin layer of vitrified buffer is a more gentle preparation procedure and most likely preserves the molecules in their native state. These samples can be imaged under low dose conditions in an electron microscope at temperatures between −160°C and −180°C reducing the effects of beam damage. The contrast of the resulting image is merely a phase contrast between molecules of very similar electron density, i.e. between water, protein and lipid. Fig. 6 shows an electron micrograph of CF_0F reconstituted in phosphatidylcholine liposomes with approx. 50 CF_0F_1 per liposome [40]. The
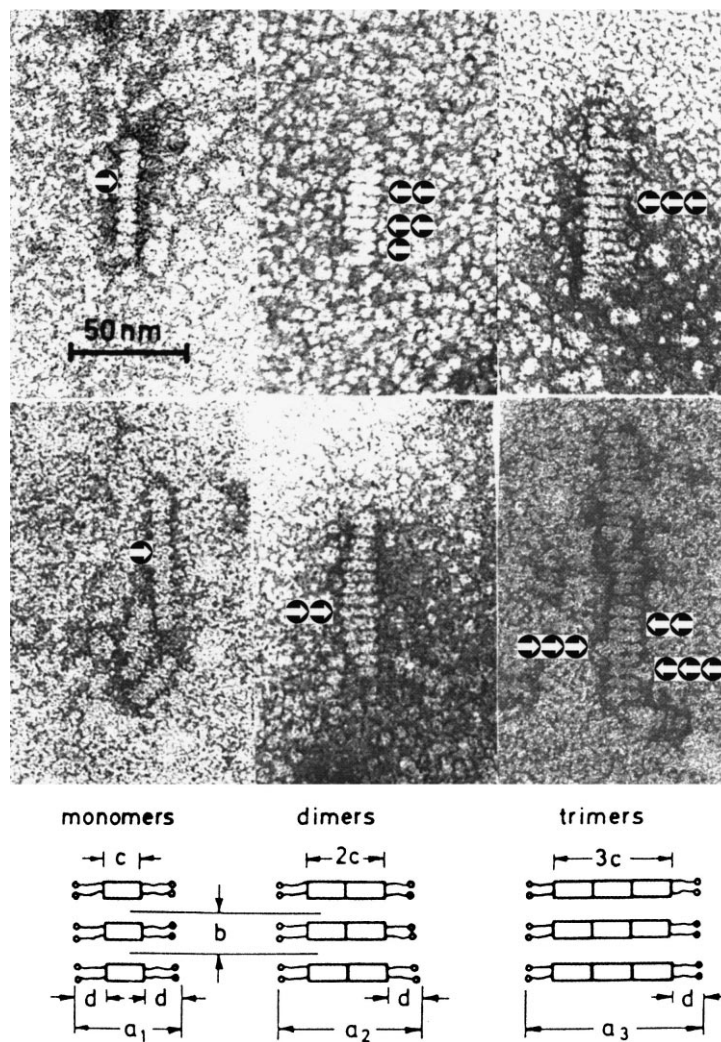
Fig. 5. Selected parts of electron micrographs of the subunit III complex. The subunit III complex shows two different types of aggregation. Along the vertical stack axis there is an interaction of the hydrophilic domains as indicated by the stain accessible cleft between the complexes. Along the horizontal axis there is hydrophobic interaction between the complexes resulting in an aggregation without a cleft. The interpretation of the structure is shown below [9].

vesicles show spherical projections with diameters between 20 and 200 nm. The outer edge of the vesicle projections has a bilayer structure. At the border of the vesicles darker lollipop-like structures are projecting out of the membrane. A small stalk connects the spherical part of the lollipop to the membrane. These structures were interpreted as side-view projections of the CF_0F_1. For image analysis a data set of 483 individual projections showing CF_0F_1 in vesicles in side-view position was used. This data set was aligned to a common reference. Fig. 7 shows the average image of the H^+-ATPase in a side-view projection. The molecule consists of three structural parts: the membrane integrated F_0 moiety (in the membrane), a small stalk projecting out of the F_0 moiety and the spherical F_1 moiety (in an aqueous environment). The mass distribution inside the CF_1 moiety is not homogeneous. The lowest mass density is observed in the middle of the CF_1 moiety. There are two similar centres of higher densities inside the F_1 moiety, which are elongated with their long axis perpendicular to the plane of the membrane. The CF_0 part can be seen in the lipid bilayer. The diameter of the CF_0 part cannot be determined from this figure since the averaging procedure combines different views of the asymmetrical CF_0 part. Full ATP synthesis activity was demonstrated for the reconstituted CF_0F_1 after freezing and thawing. This indicates that

Fig. 6. Electron micrographs of CF_0F_1 reconstituted into phosphatidylcholine liposomes in vitrified ice. CF_0F_1 can be seen in a side-view projection at the vesicle membrane and in a top-view and bottom-view projection in the centre of the vesicles [40].

electron cryomicroscopy measures a functional active enzyme [40].

CF_0F_1 can be aggregated in two-dimensional ordered arrays ('two-dimensional crystals'). These arrays were investigated by electron cryomicroscopy (see Fig. 8, top) and the signal-to-noise ratio was improved by image analysis. Fig. 8, bottom, shows the result of such an analysis [41]. This image is a projection through the holoenzyme and it is, therefore, not possible to say which part of the density in the average image results from which subunit. However, we can compare the structure of negatively stained CF_1 (see Fig. 2C) with that of the CF_0F_1 crystals (Fig. 8, bottom). It is evident from this comparison that CF_1 appears to be rather 6-fold symmetric and that the attachment of CF_0 leads to a strong asymmetry of the molecule. This might be due either to a rearrangement of the α- and β-subunits when CF_0 is attached to CF_1, or it reflects the asymmetric positioning and structure of CF_0. Possibly, both effects might play a role.

For the isolated F_1, it was shown that during hydrolysis the central γ-subunit rotates with respect to the α- and β-subunits [59–62]. The ε-subunit was shown to rotate together with the γ-subunit. This was concluded from the results of cross-link experiments in EF_0F_1, where cross-linking of the ε- and γ-

subunits had no influence on Mg^{2+}-ATPase activity [63], from cross-link experiments in EF_1, where the γ- and ε-subunits are shown to be essentially randomly distributed between the α-subunits [64] and from direct observation of the rotation with single molecules [65]. The structural and functional data were combined in a tentative model in which the rotating portion ('rotor') is formed by the γ- and ε-subunits and a complex of 12 copies of subunit III. The static part ('stator') is formed by subunits I, II and δ and the $(\alpha\beta)_3$ complex [66].

The rotor-stator concept requires two stalks connecting F_1 to F_0. To check whether evidence for a second stalk can be found, we reinvestigated CF_0F_1 preparations by electron microscopy and image processing of negatively stained samples [42]. We prepared a monodisperse sample of CF_0F_1. About 4750 individual CF_0F_1 particles from 72 different micrographs were aligned to a common reference and classified using multivariate statistical analysis and then a multi-reference alignment was carried out [54–57]. Alignment and classification steps were repeated until no further improvement was observed. All class averages show a larger F_1 and a smaller F_0 domain separated by a gap. The F_0 part has a compact appearance with a width of about 9.2 nm and a height of 8.2 nm. It might still be surrounded by a

detergent micelle. Therefore, the measured width of F_0 could be overestimated. The different class averages represent different projections of the enzyme and some of them show two stalks. One class average, which shows the largest separation between the two stalks, is shown in Fig. 9, left. One of the two stalks has a higher density. It connects the central part of F_1 to a part slightly out of centre in F_0. The central origin of this stalk in F_1 is consistent with the protruding part of the γ-subunit in the atomic model of mitochondrial MF_1 [2]. It is concluded from cross-link experiments that this stalk is formed by the γ- and ε-subunits [63] and is connected to the subunit III complex [67,68], which would be consistent with a place slightly out of the centre of F_0. According to the model proposed by Engelbrecht

Fig. 8. Ordered two-dimensional array of CF_0F_1 in vitrified ice. (Top) Electron micrograph. (Bottom) Top-view projection of CF_0F_1. Data from 30 fragments from ordered arrays were oriented and averaged [41].

and Junge [66], this stalk would form part of the rotor of the H^+-ATPase.

The other stalk is less prominent and connects a peripheral part of F_1 to a peripheral part of F_0 (see Fig. 9, left). It is presumably formed by subunits δ, I and II. Atomic force microscopy [36,37] and electron microscopy [35] on EF_0 indicate that subunits I and II (the two b-subunits) are located at the outside of the subunit III complex (subunit c) at the periphery of F_0, which is consistent with the peripheral location of the outer stalk in F_0. The δ-subunit can be cross-linked to $(αβ)_3$ in the upper outer third of F_1 [69]. The second stalk in the class average shown in Fig. 9 connects F_0 to a peripheral part of F_1, but cannot be traced to the upper part of F_1. A possible explanation could be a close interaction between the stalk and the $(αβ)_3$ complex, which would result in projections in which F_1 and the outer stalk overlap. The main distances in this average image are summarised in Fig. 9, left. The two stalks are approx. 3.3 nm
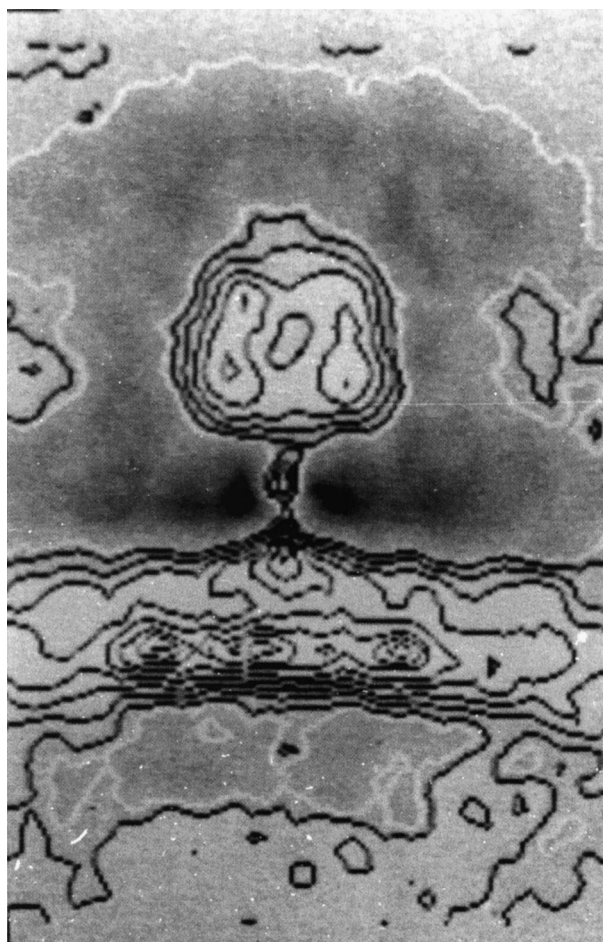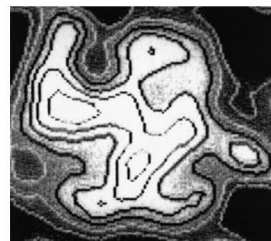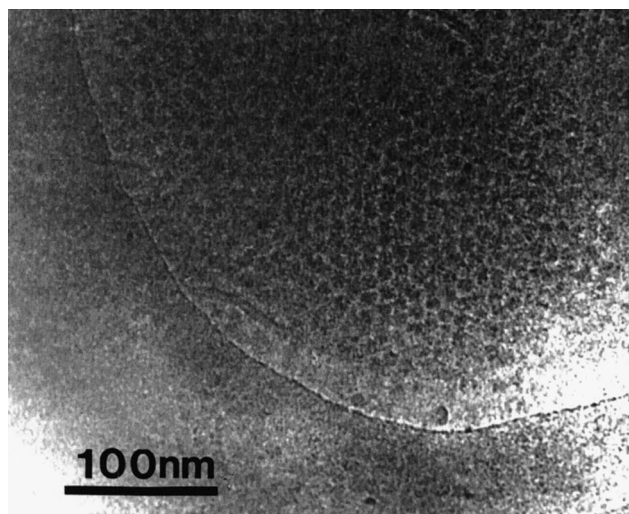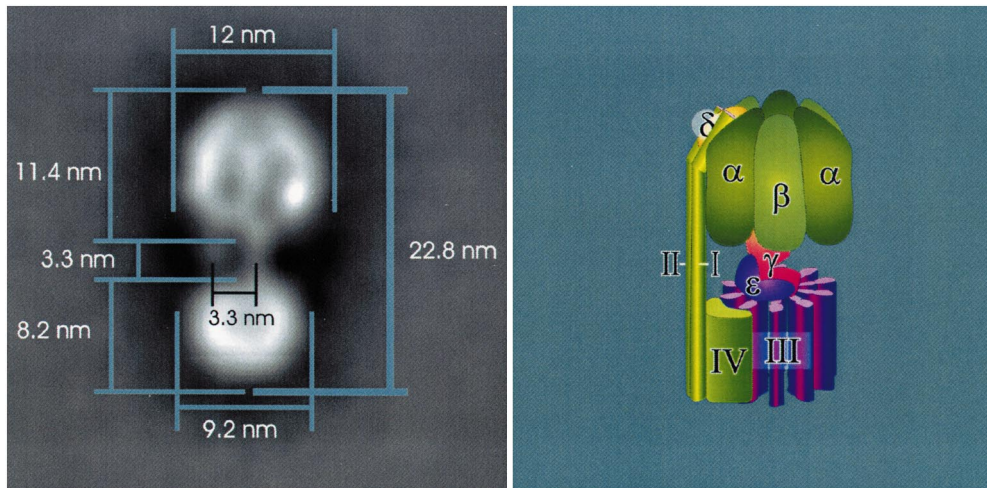

Fig. 7. Structure of CF_0F_1 in the liposome membrane. With 483 side-view projections an average image was calculated [40]. The average image shows clearly the CF_1 part and the stalk. Within the liposome membrane the CF_0 part can be seen.

Fig. 9. Side-view projection of CF_0F_1 showing two stalks. (Left) Class average displaying the largest separation of the two stalks. This class contains 270 particles out of 4750 used for classification. The dimensions of the enzyme are indicated [42]. (Right) Schematic interpretation of the structure based on electron microscopic and biochemical data.

apart, which is roughly half the diameter of the subunit III complex [9]. A schematic interpretation of the results from electron microscopy based on the biochemical data discussed above is given in Fig. 9, right.

The stalk region comprises a relatively weak density compared to the large and small domain. Therefore, classification is much more influenced by the modulation in the F_1 part than by different arrangements in the stalk region. Hence classification was
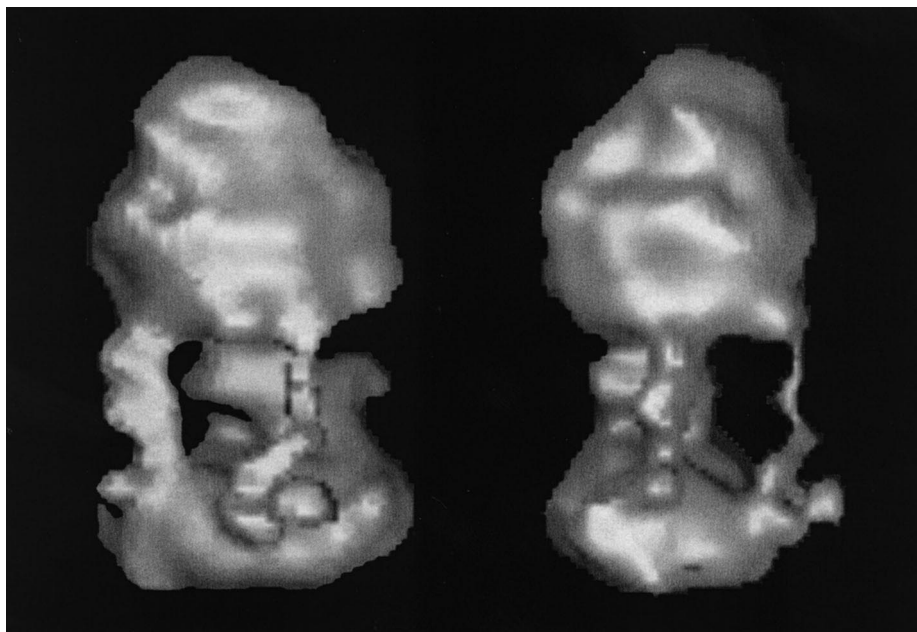

Fig. 10. Three-dimensional view of EF_0F_1. The images of about 5000 EF_0F_1 molecules were collected and a multi-reference alignment was carried out. The spatial relation between the class averages was determined by sinograms [70] and a three-dimensional map was calculated. A surface representation of the three-dimensional map is shown with different directions of the view [71]. Rotation was carried out around a vertical axis running through the centre of EF_0F_1. The view on the left was obtained by a 60° counterclockwise rotation of the view on the right.

repeated, limiting the area for classification either to the stalk region or to the whole enzyme. It is important to note that similar results are obtained independent of the chosen area of classification. The different appearances of the class averages, especially the observation of one or two stalks, are most likely due to different side-view projections of CF_0F_1. Side-view orientations can be expected where the two stalks overlap in projection and appear to form a single stalk [42]. In earlier investigations on CF_0F_1 [40], particles were aligned and averaged with no further classification. Under these circumstances an asymmetric weak feature like the second stalk would just average out if the particle can have different side-view orientations. Indeed, if an average of all particles presented here is calculated, the result is very similar to the 'old' data (Fig. 7), showing no second stalk. Consequently, the detection of the second stalk is less a question of the parameters chosen for the classification than for doing a classification at all. Therefore, we conclude that the second stalk is a genuine feature of CF_0F_1. This is in agreement with other findings from electron microscopic investigations of EF_0F_1 [34] and MF_0F_1 [52].

Recently, we have investigated the isolated H^+-ATPase from *E. coli* (EF_0F_1) by electron microscopy of samples of negatively stained monodisperse molecules. The class averages were calculated by single particle image processing as described above. In addition, the spatial relation between the class averages was determined using sinograms [70], and a three-dimensional map of EF_0F_1 was calculated [71].

Fig. 10 shows a surface representation of the three-dimensional map in two different views. The view on the left is rotated by 60° counterclockwise with respect to the view on the right around the vertical axis through the centre of EF_0F_1. The resulting surface representations in Fig. 10 show an asymmetric particle. The F_0 part is slightly elongated in one direction. Since F_0 is likely to be surrounded by a micellar arrangement of detergent molecules, its dimension is probably overestimated by up to 4–5 nm (see Figs. 4 and 5). These results support the current view of the F_0 structure with the a- and b-subunits attached to a ring of a subunit c complex at one side. This is in accordance with the results from atomic force microscopy experiments on EF_0 [36,37].

Most interestingly, at this contour level three connections between the F_0 part and the F_1 part become
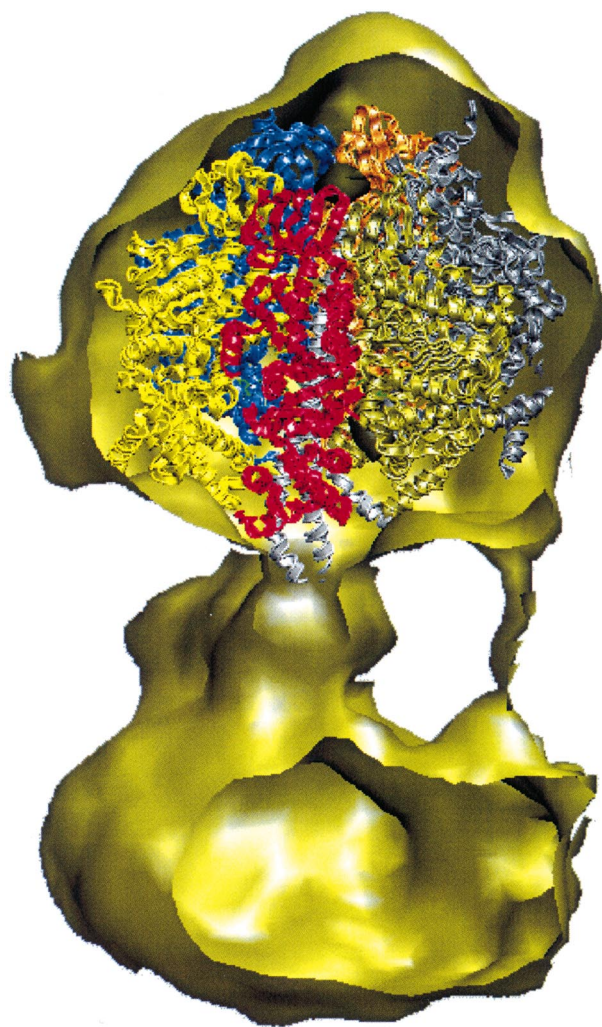

Fig. 11. Comparison of electron microscopic data from EF_0F_1 to the X-ray structure of MF_1. A similar three-dimensional view is shown as in Fig. 10, right. In the three-dimensional map, the front surface of the enzyme was removed and the MF_1 structure placed into the EF_1 part [71].

visible. The thick central stalk had an oval cross-section and was built of two distinct parts, one closer to the base of F_1, the other part closing the cavity in the F_0 moiety. It is widely agreed that the stalk is formed by subunits ε and γ [63–65]; this assignment is consistent with the position of the two areas of higher density between the F_1 and F_0 part observed in our maps. The ε-subunit would then correspond to the region of density closer to the F_0 part as indicated by cross-link experiments [63,72]. The second smaller connection between F_0 and F_1 which probably forms the stator can only be detected with confidence when a classification of the F_0F_1 images is

carried out (see Fig. 9). It is assumed that this structural element is partly formed by the b-subunits. Since there are two of these subunits per EF_0F_1 complex, one possibility would be that the second stalk consists of two of these subunits. When the three-dimensional reconstruction was calculated from the electron microscopic data, a third connecting element becomes visible between the F_1 and F_0 part which was smaller than the second stalk. In Fig. 10, right, the third connection is seen on the right, in Fig. 10, left, it is seen at the front. This tiny third stalk is formed presumably by a single α-helix. Such a small structural detail can only be detected under exceptionally favourable circumstances in negatively stained samples at this level of resolution. It is almost more surprising to detect this kind of detail at all than missing it out. Therefore, this observation must be further investigated by biochemical methods, before conclusions concerning the mechanism of the enzyme can be drawn. Currently, we have no hint which subunit might form the third stalk. This encourages new speculations on the structural arrangement of the different subunits for the 'stator' elements.

In Fig. 11 a similar view is shown as in Fig. 10, right. For comparison with the high resolution structure of MF_1, the front surface of the image of EF_0F_1 was removed and the MF_1 structure was placed in the F_1 part of the holoenzyme. The X-ray structure of MF_1 fits reasonably well with the F_1 part of the *E. coli* ATPase. The small differences might be due to several effects, first of all there might exist species-specific differences, second in the MF_1 structure information on δ, ε, parts of γ and the N-terminal ends of α and β are missing, and third, in order to obtain information on very tiny structures, the contour line of the three-dimensional map has been chosen near to the noise level. Presumably, the latter effect is responsible for most of the observed differences. Therefore, the electron microscopic data at this contour level overestimate the size.

It should be mentioned that, recently, a third connection between the F_0 part and the F_1 part has also been reported for V-type ATPases [73]. Thus, the structural connection between the two parts of the F-type and V-type ATPases seems to be more complex than previously thought.

5. Note added in proof

Recently an electron density map obtained by X-ray analysis of the yeast mitochondrial H^+-ATPase subcomplex has been reported and the subunit c-complex shows a ring of 10 c-subunits [74,75]. The subunit III-complex of the H^+-ATPase from chloroplasts was investigated with atomic-force-microscopy. In this work, a ring structure of the subunit III-complex with 14 III-subunits was observed.

Acknowledgements

References

[1] P. Mitchell, Nature 191 (1961) 144.

[2] J.P. Abrahams, A.G.W. Leslie, R. Lutter, J.E. Walker, Nature 370 (1994) 621–628.

[3] N. Nelson, H. Nelson, E. Racker, J. Biol. Chem. 247 (1972) 7657–7662.

[4] K.H. Süss, O. Schmidt, FEBS Lett. 144 (1982) 213.

[5] J.V. Moroney, L. Lopresti, B.F. McEwen, R.E. McCarty, G.G. Hammes, FEBS Lett. 158 (1983) 58.

[6] U. Pick, E. Racker, J. Biol. Chem. 254 (1979) 2793–2799.

[7] P. Fromme, P. Gräber, J. Salnikov, FEBS Lett. 218 (1987) 27–30.

[8] K. Sigrist-Nelson, H. Sigrist, A. Azzi, Eur. J. Biochem. 92 (1978) 9–14.

[9] P. Fromme, E.J. Boekema, P. Gräber, Z. Naturforsch. 42c (1987) 1239–1245.

[10] D.L. Foster, R.H. Fillingame, J. Biol. Chem. 257 (1982) 2009–2015.

[11] P.C. Jones, R.H. Fillingame, J. Biol. Chem. 273 (1998) 29701–29705.

[12] J. Hennig, R.G. Herrmann, Mol. Gen. Genet. 203 (1986) 117–128.

[13] A.L. Cozens, J.E. Walker, A.L. Phillips, A.K. Muttly, J.c. Gray, EMBO J. 5 (1986) 217–222.

[14] G. Groth, K. Schirwitz, Eur. J. Biochem. 260 (1999) 15–21.

[15] G.L. Orris, A.G. Leslie, K. Braig, J.E. Walker, Structure 15 (1998) 831–837.

[16] M.J. van Raaij, G.L. Orriss, M.G. Montgomery, M.J. Runswick, I.M. Fearnley, J.M. Skehel, J.E. Walker, Biochemistry 35 (1996) 15618–15625.

[17] J.P. Abrahams, S.K. Buchanan, M.J. van Raaij, I.M. Fearnley, A.G. Leslie, J.E. Walker, Proc. Natl. Acad. Sci. USA 93 (1996) 9420–9424.

[18] M.J. van Raaij, J.P. Abrahams, A.G. Leslie, J.E. Walker, Proc. Natl. Acad. Sci. USA 93 (1996) 6913–6917.

[19] M. Bianchet, X. Ysern, J. Hullihen, P.L. Pedersen, L.M. Amzel, J. Biol. Chem. 266 (31) (1991) 21197–21201.

[20] Y. Shirakihara, A.G. Leslie, J.P. Abrahams, J.E. Walker e, T. Ueda, Y. Sekimoto, M. Kambara, K. Saika, Y. Kagawa, M. Yoshida, Structure 15 (1997) 825–836.

[21] S. Wilkens, F.W. Dahlquist, L.P. McIntosh, K.W. Donaldson, R.A. Capaldi, Nat. Struct. Biol. 2 (1995) 961–967.

[22] S. Wilkens, R.E. Capaldi, J. Biol. Chem. 273 (1998) 26645–26651.

[23] U. Uhlin, G.B. Cox, J.M. Guss et al., Structure 5 (1997) 1219–1230.

[24] S. Wilkens, A. Rodgers, I. Ogilvie, R.A. Capaldi, Biophys. Chem. 68 (1997) 95–102.

[25] O. Dmitriev, P.C. Jones, W. Jiang, R.H. Fillingame, J. Biol. Chem. 274 (1999) 15598–15604.

[26] Y. Oleg, O. Dmitriev, P.C. Jones, R.H. Fillingame, Biochemistry 96 (1999) 7785–7790.

[27] M.E. Girwin, V.K. Rastogi, F. Abildgaard, J.L. Markley, R.H. Fillingame, Biochemistry 37 (1998) 8817–8824.

[28] U. Matthey, G. Kaim, D. Braun, K. Wüthrich, P. Dimroth, Eur. J. Biochem. 261 (1999) 459–467.

[29] E.P. Gogol, E. Johnston, R. Aggeler, R.A. Capaldi, Proc. Natl. Acad. Sci. USA 87 (24) (1990) 9585–9589.

[30] S. Wilkens, R.A. Capaldi, FEBS Lett. 354 (1994) 37–40.

[31] E.P. Gogol, U. Lücken, T. Bork, R.A. Capaldi, Biochemistry 28 (1989) 4717–4724.

[32] E.P. Gogol, U. Lücken, R.A. Capaldi, FEBS Lett. 219 (1987) 274–278.

[33] U. Lücken, E.P. Gogol, R.A. Capaldi, Biochemistry 29 (1990) 5339–5343.

[34] S. Wilkens, R.A. Capaldi, Biochim. Biophys. Acta 1365 (1998) 93–97.

[35] R. Birkenhäger, M. Hoppert, G. Deckers-Hebestreit, F. Mayer, K. Altendorf, Eur. J. Biochem. 230 (1995) 58–67.

[36] S. Singh, P. Turina, C.J. Bustamante, D.J. Keller, R. Capaldi, FEBS Lett. 297 (1996) 30–34.

[37] K. Takeyasu, H. Omote, S. Nettikadan, F. Tokumasu, A. Iwamoto-Kihara, M. Futai, FEBS Lett. 392 (1996) 110–113.

[38] D. Neff, S. Tripathi, K. Middendorf, H. Stahlberg, H.-J. Butt, E. Bamberg, N.A. Dencher, J. Struct. Biol. 119 (1997) 139–148.

[39] E.J. Boekema, G. Schmidt, P. Gräber, J.A. Berden, Z. Naturforsch. 43c (1988) 219.

[40] B. Böttcher, U. Lücken, P. Gräber, Biochem. Soc. Trans. 23 (1995) 780–785.

[41] B. Böttcher, P. Gräber, E.J. Boekema, U. Lücken, FEBS Lett. 373 (1995) 262–264.

[42] B. Böttcher, L. Schwarz, P. Gräber, J. Mol. Biol. 281 (1998) 757–762.

[43] E.J. Boekema, M. van Heel, P. Gräber, Biochim. Biophys. Acta 933 (1988) 365–371.

[44] E.J. Boekema, J. Xiao, R.E. McCarty, Biochim. Biophys. Acta 1020 (1990) 49–56.

[45] E.J. Boekema, B. Böttcher, Biochim. Biophys. Acta 1098 (1992) 131–143.

[46] C.W. Akey, R.H. Crepeau, S.D. Dunn, R.E. McCarty, S.J. Edelstein, EMBO J. 2 (1983) 1409–1415.

[47] H. Tiedge, H. Lünsdorf, G. Schäfer, H.U. Schairer, Proc. Natl. Acad. Sci. USA 82 (1985) 7874–7878.

[48] V.L. Tsuprun, I.V. Mesyanzhinova, I.A. Kozlov, E.V. Orlova, FEBS Lett. 167 (1984) 285–290.

[49] J. Boekema, J.A. Berden, M.G. van Heel, Biochim. Biophys. Acta 851 (1986) 353–360.

[50] J.W. Soper, G.L. Decker, P.L. Pedersen, J. Biol. Chem. 254 (1979) 11170.

[51] E. Mörschel, L.A. Staehelin, J. Cell Biol. 97 (1983) 301.

[52] S. Karrasch, J.E. Walker, J. Mol. Biol. 290 (1999) 379–384.

[53] R.E. McCarty, E. Racker, Brookhaven Symp. Biol. 19 (1966) 202–214.

[54] M. van Heel, J. Frank, Ultramicroscopy 6 (1981) 187–194.

[55] M. van Heel, Optik 82 (1989) 114–126.

[56] M. van Heel, M. Stöffler-Meilicke, EMBO J. 4 (1985) 2389–2395.

[57] L. Borland, M. van Heel, J. Optic. Soc. Am. Ser. A 7 (1990) 601–610.

[58] I. Grotjohann, P. Gräber, Biochim. Biophys. Acta 1017 (1990) 177–180.

[59] T.M. Duncan, V.V. Bulygin, Y. Zhou, M.L. Hutcheon, R.L. Cross, Proc. Natl. Acad. Sci. USA 92 (1995) 10964–10968.

[60] D. Sabbert, S. Engelbrecht, W. Junge, Nature 381 (1996) 623–626.

[61] H. Noji, R. Yasuda, M. Yoshida, K. Kinosita Jr., Nature 386 (1997) 299–302.

[62] D. Sabbert, S. Engelbrecht, W. Junge, Proc. Natl. Acad. Sci. USA 94 (1997) 4401–4405.

[63] B. Schulenberg, F. Wellmer, H. Lill, W. Junge, S. Engelbrecht, Eur. J. Biochem. 249 (1997) 134–141.

[64] R. Aggeler, I. Ogilvie, R.A. Capaldi, J. Biol. Chem. 272 (1997) 19621–19624.

[65] Y. Kato-Yamada, H. Noji, R. Yasuda, K. Kinosita Jr., M. Yoshida, J. Biol. Chem. 273 (1998) 19375–19377.

[66] S. Engelbrecht, W. Junge, FEBS Lett. 414 (1997) 485–491.

[67] Y. Zhang, R.H. Fillingame, J. Biol. Chem. 270 (1995) 24609–24614.

[68] S.D. Watts, C. Tang, R.A. Capaldi, J. Biol. Chem. 271 (1996) 28341–28347.

[69] H. Lill, F. Hensel, W. Junge, S. Engelbrecht, J. Biol. Chem. 271 (1996) 32737–32742.

[70] M. van Heel, Ultramicroscopy 21 (1987) 111–124.

[71] B. Böttcher, I. Bertsche, R. Reuter, P. Gräber, J. Mol. Biol. (1999) in press.

[72] J. Hermolin, O.Y. Dimitriev, Y. Zhang, R.H. Fillingame, J. Biol. Chem. 274 (1999) 17011–17016.

[73] E.J. Boekema, J.F.L. van Breemen, A. Birsson, T. Ubbink-kok, W.N. Konigs, J.S. Lolkema, Nature 401 (1999) 37–38.

[74] D. Stock, A.G.W. Leslie, J.E. Walker, Science 286 (1999) 1700–1705.

[75] H. Seelert, A. Poetsch, N.A. Dencher, A. Engel, H. Stahlberg and D.J. Müller (2000) Nature, in press.